

NP-Match: Towards a New Probabilistic Model for Semi-Supervised Learning

Jianfeng Wang, Xiaolin Hu, *Senior Member, IEEE*, and Thomas Lukasiewicz

Abstract—Semi-supervised learning (SSL) has been widely explored in recent years, and it is an effective way of leveraging unlabeled data to reduce the reliance on labeled data. In this work, we adjust neural processes (NPs) to the semi-supervised image classification task, resulting in a new method named NP-Match. NP-Match is suited to this task for two reasons. Firstly, NP-Match implicitly compares data points when making predictions, and as a result, the prediction of each unlabeled data point is affected by the labeled data points that are similar to it, which improves the quality of pseudo-labels. Secondly, NP-Match is able to estimate uncertainty that can be used as a tool for selecting unlabeled samples with reliable pseudo-labels. Compared with uncertainty-based SSL methods implemented with Monte-Carlo (MC) dropout, NP-Match estimates uncertainty with much less computational overhead, which can save time at both the training and the testing phases. We conducted extensive experiments on five public datasets under three semi-supervised image classification settings, namely, the standard semi-supervised image classification, the imbalanced semi-supervised image classification, and the multi-label semi-supervised image classification, and NP-Match outperforms state-of-the-art (SOTA) approaches or achieves competitive results on them, which shows the effectiveness of NP-Match and its potential for SSL.

Index Terms—Neural Processes, NP-Match, Semi-Supervised Image Classification, Imbalanced Semi-Supervised Image Classification, Multi-Label Semi-Supervised Image Classification

1 INTRODUCTION

DEEP neural networks have been widely used in computer vision tasks [1], [2], [3], [4], [5], [6] due to their strong performance. Training deep neural networks relies on large-scale labeled datasets, but annotating large-scale datasets is time-consuming, which encourages researchers to explore semi-supervised learning (SSL). SSL aims to learn from few labeled data and a large amount of unlabeled data, and it has been a long-standing problem in computer vision and machine learning [7], [8], [9], [10], [11], [12], [13], [14]. In this work, we focus on SSL for image classification.

Most recent approaches to SSL for image classification are based on the combination of consistency regularization and pseudo-labeling [7], [8], [9], [10], [15], [16], [17]. They can be further classified into two categories, namely, deterministic [7], [8], [10], [15], [16], [17] and probabilistic ones [9]. A deterministic approach aims at directly making predictions, while a probabilistic approach tries to additionally model the predictive distribution, such as using Bayesian neural networks, which are implemented by Monte-Carlo (MC) dropout [18]. As a result, the former cannot estimate the uncertainty of the model’s prediction, and unlabeled samples are selected only based on high-confidence predictions. In contrast, the latter can give uncertainties for unlabeled samples, and the uncertainties can be combined with high-

confidence predictions for picking or refining pseudo-labels.

Current SOTA methods for the semi-supervised image classification task are deterministic, including FixMatch [7], CoMatch [15], and FlexMatch [8], which have achieved promising results on public benchmarks. In contrast, progress on probabilistic approaches lags behind, which is mainly shown by the fact that there are only few studies on this task and MC dropout becomes the only option for implementing the probabilistic model [9]. In addition, MC dropout also dominates the uncertainty-based approaches to other SSL tasks [19], [20], [21], [22], [23], [24]. MC dropout, however, is time-consuming, requiring several feedforward passes to get uncertainty at both the training and the test stages, especially when some large models are used.

To solve this drawback and to further promote related research, we need to find better probabilistic approaches for SSL. Considering that MC dropout is an approximation to the Gaussian process (GP) model [18], we turn to another approximation model called neural processes (NPs) [25], which can be regarded as a neural-network-based formulation that approximates GPs. Similarly to a GP, an NP is also a probabilistic model that defines distributions over functions. Thus, an NP is able to rapidly adapt to new observations, with the advantage of estimating the uncertainty of each observation. There are two main aspects that motivate us to investigate NPs in SSL. Firstly, GPs have been preliminarily explored for some SSL tasks [26], [27], [28], because of the property that their kernels are able to compare labeled data with unlabeled data when making predictions. NPs share this property, since it has been proved that NPs can learn non-trivial implicit kernels from data [25]. As a result, NPs are able to make predictions for target points conditioned on context points. This feature is highly relevant to SSL, which must learn from limited labeled samples to make predictions

- Jianfeng Wang is with the Computer Science Department, University of Oxford, United Kingdom. E-mail: jianfeng.wang@cs.ox.ac.uk.
- Xiaolin Hu is with the Institute for Artificial Intelligence, the State Key Laboratory of Intelligent Technology and Systems, Beijing National Research Center for Information Science and Technology, and Department of Computer Science and Technology, Tsinghua University, Beijing, China. E-mail: xlhu@tsinghua.edu.cn.
- Thomas Lukasiewicz is with the Institute of Logic and Computation, TU Wien, Austria, and the Computer Science Department, University of Oxford, United Kingdom. E-mail: thomas.lukasiewicz@cs.ox.ac.uk.

for unlabeled data, similarly to how NPs are able to impute unknown pixel values (i.e., target points) when given only a small number of known pixels (namely, context points) [25]. Due to the learned implicit kernels in NPs [25] and the successful application of GPs to different SSL tasks [26], [27], [28], NPs could be a suitable probabilistic model for SSL, as the kernels can compare labeled data with unlabeled data to improve the quality of pseudo-labels for the unlabeled data at the training stage. Secondly, previous GP-based works for SSL do not explore the semi-supervised large-scale image classification task, since GPs are computationally expensive, which usually incur a $\mathcal{O}(n^3)$ runtime for n training points. But, unlike GPs, NPs are more efficient than GPs, providing the possibility of applying NPs to this task. NPs are also computationally significantly more efficient than current MC-dropout-based approaches to SSL, since, given an input image, they only need to perform one feedforward pass to obtain the prediction with an uncertainty estimate.

In this work, we take the first step to explore NPs in large-scale semi-supervised image classification, and propose a new probabilistic method called NP-Match. NP-Match still rests on the combination of consistency regularization and pseudo-labeling, but it incorporates NPs to the top of deep neural networks, and therefore it is a probabilistic approach. Compared to the previous probabilistic method for semi-supervised image classification [9], NP-Match not only can make predictions and estimate uncertainty more efficiently, inheriting the advantages of NPs, but also can achieve a better performance on public benchmarks.

Summarizing, the main contributions are:

- We propose NP-Match, which adjusts NPs to SSL, and explore its use in semi-supervised large-scale image classification. To our knowledge, this is the first such work. In addition, NP-Match has the potential to break the monopoly of MC dropout as the probabilistic model in SSL.
- We experimentally show that the Kullback-Leibler (KL) divergence in the evidence lower bound (ELBO) of NPs [25] is not a good choice in the context of SSL, which may negatively impact the learning of global latent variables. To tackle this problem, we propose a new uncertainty-guided skew-geometric Jensen-Shannon (JS) divergence ($JS^{G_{\alpha_u}}$) for NP-Match.
- We show that NP-Match outperforms SOTA results or achieves competitive results on public benchmarks, demonstrating its effectiveness for SSL. We also show that NP-Match estimates uncertainty faster than the MC-dropout-based probabilistic model, which can improve the training and the test efficiency.

Some preliminary results have been presented at a conference [29], and we extend the previous work [29] by introducing more experiments on two new tasks. First, we supplement experiments on imbalanced semi-supervised image classification, which is more challenging, since deep models may overfit to frequent classes, leading to inaccurate pseudo-labels. Accordingly, we also present related works in this field. Second, we add additional results on another important task, i.e., multi-label semi-supervised image classification. Multi-label classification increases the risk of making wrong predictions for unlabeled data, therefore offering a more tough and realistic scenario for evaluating our model.

As the uncertainty estimation is vital in safety-critical areas, such as medical applications, we choose a Chest X-Ray dataset as our multi-label classification benchmark. The new experiments and analysis provide a more solid evidence to justify our claim and contributions.

The rest of this paper is organized as follows. In Section 2, we review related methods. Section 3 presents NP-Match and the uncertainty-guided skew-geometric JS divergence ($JS^{G_{\alpha_u}}$), followed by the experimental settings and results in Section 4. In Section 5, we give a summary and an outlook on future research. The source code is available at: <https://github.com/Jianf-Wang/NP-Match>

2 RELATED WORK

We now briefly review related works, including *semi-supervised learning (SSL) for image classification*, *imbalanced semi-supervised image classification*, *Gaussian processes (GPs) for SSL*, and *neural processes (NPs)*.

SSL for image classification. Most methods for semi-supervised image classification in the past few years are based on pseudo-labeling and consistency regularization. Pseudo-labeling approaches rely on the high confidence of pseudo-labels, which can be added to the training data set as labeled data, and these approaches can be classified into two classes, namely, disagreement-based models and self-training models. The former models aim to train multiple learners and exploit the disagreement during the learning process [30], [31], while the latter models aim at training the model on a small amount of labeled data, and then using its predictions on the unlabeled data as pseudo-labels [10], [32], [33], [34]. Consistency-regularization-based approaches work by performing different transformations on an input image and adding a regularization term to make their predictions consistent [13], [35], [36], [37], [38]. Based on these two approaches, FixMatch [7] is proposed, which achieves new state-of-the-art (SOTA) results on the most commonly-studied SSL benchmarks. FixMatch [7] combines the merits of these two approaches: given an unlabeled image, weak data augmentation and strong data augmentation are performed on the image, leading to two versions of the image, and then FixMatch produces a pseudo-label based on its weakly-augmented version and a preset confidence threshold, which is used as the true label for its strongly augmented version to train the whole framework. The success of FixMatch inspired several subsequent methods [8], [9], [10], [15], [16], [17]. For instance, Li et al. [15] additionally design the classification head and the projection head for generating a class probability and a low-dimensional embedding, respectively. The projection head and the classification head are jointly optimized during training. Specifically, the former is learnt with contrastive learning on pseudo-label graphs to encourage the embeddings of samples with similar pseudo-labels to be close, and the latter is trained with pseudo-labels that are smoothed by aggregating information from nearby samples in the embedding space. Zhang et al. [8] propose to use dynamic confidence thresholds that are automatically adjusted according to the model’s learning status of each class. Rizve et al. [9] propose an uncertainty-aware pseudo-label selection (UPS) framework for semi-supervised image classification. The UPS framework introduces MC

dropout to obtain uncertainty estimates, which are then leveraged as a tool for selecting pseudo-labels. This is the first work using MC dropout for semi-supervised image classification.

Imbalanced semi-supervised image classification. Training deep neural networks requires large-scale datasets, and one fundamental characteristic of these datasets in practice is that the data distribution over different categories is imbalanced (e.g., long-tailed), as it is common that the images of some categories are difficult to be collected. Training deep models on imbalanced datasets makes the models overfit to majority classes, and several methods have been proposed to ameliorate this issue [39], [40], [41], [42], [43], [44], [45], [46], [47], [48], [49], [50], [51], [52]. According to Yang and Xu [53], semi-supervised learning benefits imbalanced learning, as using extra data during training can reduce label bias, which greatly improves the final classifier. Therefore, imbalanced semi-supervised image classification has been drawing extensive attention in recent years. Specifically, Hyun et al. [54] analyze how class imbalance affects SSL by looking into the topography of the decision boundary, and then they propose a suppressed consistency loss (SCL) to suppress the influence of consistency loss on infrequent classes. Kim et al. [55] design an iterative procedure, called distribution aligning refinery of pseudo-labels (DARP), to solve a convex optimization problem that aims at refining biased pseudo-labels so that their distribution can match the true class distribution of unlabeled data. Wei et al. [56] introduce a class-rebalancing selftraining scheme (CRest) to re-sample pseudo-labeled data and to add them into the labeled set, for refining the whole model. Inspired by the concept of decoupled learning [57], namely, training a feature extractor and a classifier separately, He et al. [58] propose a bi-sampling method, which integrates two data samplers with various sampling strategies for decoupled learning, therefore benefiting both the feature extractor and the classifier. Lee et al. [59] design an auxiliary balanced classifier (ABC) that is trained by using a mask that re-balances the class distribution within every mini-batch. Besides, Oh et al. [60] solve the imbalanced semi-supervised image classification problem by proposing a new framework called distribution-aware semantics-oriented (DASO) pseudo-labels. DASO focuses on debiasing pseudo-labels through blending two complementary types of pseudo-labels, which enables the framework to deal with the imbalanced semi-supervised image classification task, even when the class distribution of unlabeled data is inconsistent with that of labeled data. In this work, we evaluate our method for imbalanced semi-supervised image classification based on the DASO framework.

GPs for SSL. Since NPs are also closely related to GPs, we review the application of GPs to different SSL tasks in this part. GPs, which are non-parametric models, have been preliminarily investigated in different semi-supervised learning tasks. For example, Sindhwani et al. [26] introduce a semi-supervised GP classifier, which incorporates the information of relationships among labeled and unlabeled data into the kernel. Their approach, however, has high computational costs and is thus only evaluated for a simple binary classification task on small datasets. Deep kernel learning [61] also lies on the spectrum between neural

networks and GPs, and has been integrated into a new framework for the semi-supervised regression task, named semi-supervised deep kernel learning [27], which aims to minimize the predictive variance for unlabeled data, encouraging unlabeled embeddings to be near labeled embeddings. Semi-supervised deep kernel learning, however, has not been applied to semi-supervised image classification, and (similarly to semi-supervised GPs) also comes with a high (cubic) computational complexity. Recently, Yasarla et al. [28] propose to combine GPs with UNet [62] for SSL image deraining. Here, GPs are used to get pseudo-labels for unlabeled samples based on the feature representations of labeled and unlabeled images. GPs have also been combined with graph convolutional networks for semi-supervised learning on graphs [63], [64], [65]. Although many previous works explore GPs in different semi-supervised learning tasks, none of them investigates the application of GPs to semi-supervised large-scale image classification.

NPs. The origin of NPs can be traced back to conditional NPs [66], which define conditional distributions over functions given a set of observations. Conditional NPs, however, do not introduce global latent variables for observations, which led to the birth of NPs [25]. In NPs, the mean-aggregator is used to summarize the encoded inputs of a task into a global latent variable, which is then used to make predictions on targets in the task. In recent years, several NP variants have been proposed to better approximate stochastic processes. For example, Kim et al. [67] consider that the mean-aggregator may cause difficulties for the decoder to pick relevant information with regard to making predictions, and they introduce a differentiable attention mechanism to solve this issue, resulting in new attentive NPs. Gordon et al. [68] consider that the translation equivariance is important for prediction problems, which should be considered. Therefore, they incorporate translation equivariance into NPs and design a new model, called convolutional conditional NPs. Besides, Louizos et al. [69] consider that using global latent variables is not flexible for encoding inductive biases. Thus, they propose to use local latent variables along with a dependency structure among them, resulting in new functional NPs. Lee et al. [70] point out the limitation of using a single Gaussian latent variable to model functional uncertainty. To solve the limitation, they propose to use bootstrapping for inducing functional uncertainty, leading to a new NP variant, called Bootstrapping Neural Processes (BNP). Currently, NPs and their variants have been widely used in many different settings, including meta-learning [71], [72], [73] and sequential data modelling [74], but they have not been studied in SSL. Our work is the first to leverage NPs for semi-supervised large-scale image recognition. We choose the most basic model from [25] (i.e., the original NPs), and we expect that future works can further study the application of other variants to this task.

3 METHODOLOGY

In this section, we provide a brief introduction to neural processes (NPs) and a detailed description of our NP-Match.

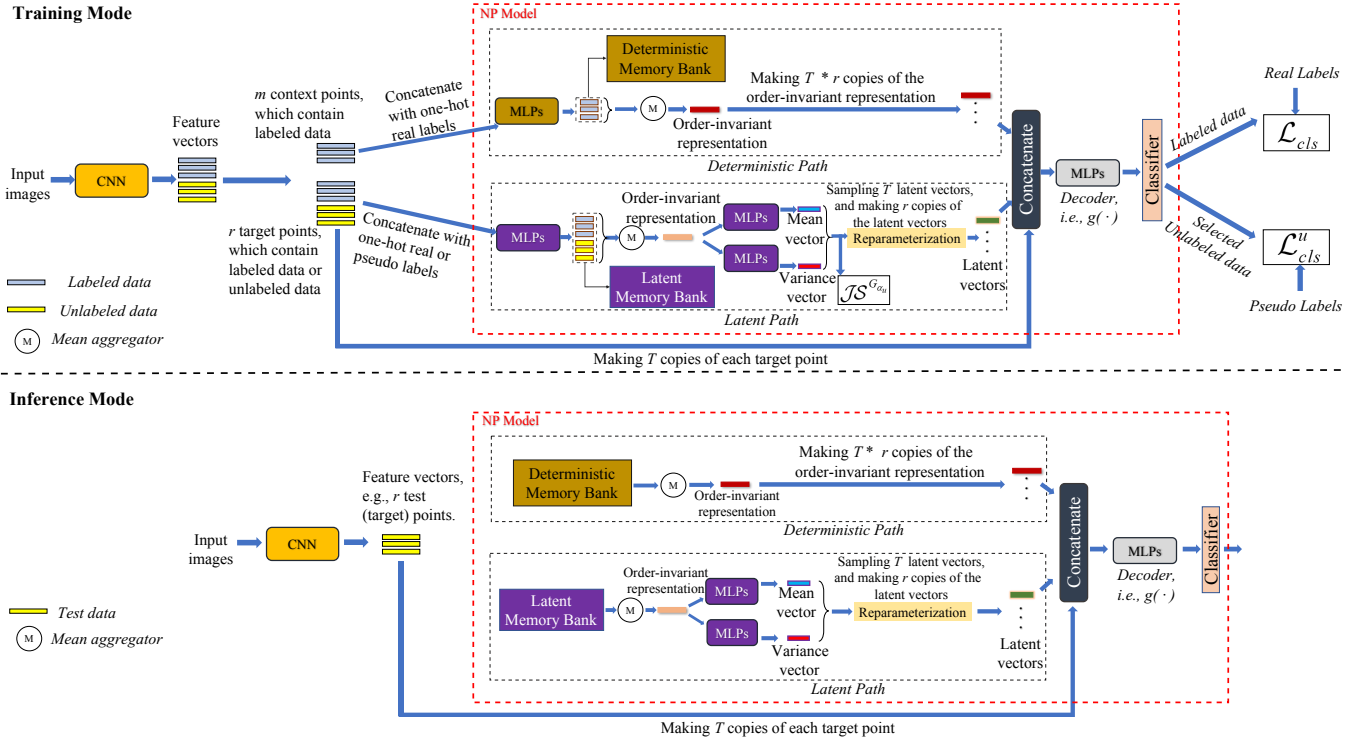


Fig. 1. Overview of NP-Match: it contains a convolutional neural network (CNN) and an NP model that is shown in the red dotted box. The feature vectors come from the global average pooling layer in the CNN.

3.1 NPs

NPs approximate stochastic processes via finite-dimensional marginal distributions [25]. Formally, given a probability space (Ω, Σ, Π) and an index set \mathcal{X} , a stochastic process can be written as $\{F(x, \omega) : x \in \mathcal{X}\}$, where $F(\cdot, \omega)$ is a sample function mapping \mathcal{X} to another space \mathcal{Y} for any point $\omega \in \Omega$. For each finite sequence $x_{1:n}$, a marginal joint distribution function can be defined on the function values $F(x_1, \omega), F(x_2, \omega), \dots, F(x_n, \omega)$, which satisfies two conditions given by the Kolmogorov Extension Theorem [75], namely, exchangeability and consistency. Assuming that a density π , where $d\Pi = \pi d\mu$, and the likelihood density $p(y_{1:n}|F(\cdot, \omega), x_{1:n})$ exist, the marginal joint distribution function can be written as:

$$p(y_{1:n}|x_{1:n}) = \int \pi(\omega) p(y_{1:n}|F(\cdot, \omega), x_{1:n}) d\mu(\omega). \quad (1)$$

The exchangeability condition requires the joint distributions to be invariant to permutations of the elements, i.e., $p(y_{1:n}|x_{1:n}) = p(\varphi(y_{1:n})|\varphi(x_{1:n}))$, where φ is a permutation of $\{1, \dots, n\}$. The consistency condition expresses that if a part of the sequence is marginalised out, then the resulting marginal distribution is consistent with that defined on the original sequence.

Letting (Ω, Σ) be $(\mathbb{R}^d, \mathcal{B}(\mathbb{R}^d))$, where $\mathcal{B}(\mathbb{R}^d)$ denotes the Borel σ -algebra of \mathbb{R}^d , NPs parameterize the function $F(\cdot, \omega)$ with a high-dimensional random vector z sampled from a multivariate Gaussian distribution. Then, $F(x_i, \omega)$ can be replaced by $g(x_i, z)$, where $g(\cdot)$ denotes a neural network, and Eq. (1) becomes:

$$p(y_{1:n}|x_{1:n}) = \int \pi(z) p(y_{1:n}|g(x_{1:n}, z), x_{1:n}) d\mu(z). \quad (2)$$

The training objective of NPs is to maximize $p(y_{1:n}|x_{1:n})$, and the learning procedure reflects the NPs' property that they have the capability to make predictions for target points conditioned on context points [25].

3.2 NP-Match

As Figure 1 shows, NP-Match is mainly composed of two parts: a deep neural network and an NP model. The deep neural network is leveraged for obtaining feature representations of input images, while the NP model is built upon the network to receive the representations for classification.

3.2.1 NP Model for Semi-supervised Image Classification

Since we extend the original NPs [25] to the classification task, $p(y_{1:n}|g(x_{1:n}, z), x_{1:n})$ in Eq. (2) should define a categorical distribution rather than a Gaussian distribution. Therefore, we parameterize the categorical distribution by probability vectors from a classifier that contains a weight matrix (\mathcal{W}) and a softmax function (Φ):

$$p(y_{1:n}|g(x_{1:n}, z), x_{1:n}) = \text{Categorical}(\Phi(\mathcal{W}g(x_{1:n}, z))). \quad (3)$$

Note that $g(\cdot)$ can be learned via amortised variational inference, and to use this method, two steps need to be done: (1) parameterize a variational distribution over z , and (2) find the evidence lower bound (ELBO) as the learning objective. For the first step, we let $q(z|x_{1:n}, y_{1:n})$ be a variational distribution defined on the same measure space, which can be parameterized by a neural network. For the second step, given a finite sequence with length n , we assume that there are m context points ($x_{1:m}$) and r target points ($x_{m+1:m+r}$)

in it, i.e., $m + r = n$. Then, the ELBO is given by (with proof in the supplementary material):

$$\begin{aligned} \log p(y_{1:n}|x_{1:n}) &\geq \\ \mathbb{E}_{q(z|x_{m+1:m+r}, y_{m+1:m+r})} &\left[\sum_{i=m+1}^{m+r} \log p(y_i|z, x_i) - \right. \\ \log \frac{q(z|x_{m+1:m+r}, y_{m+1:m+r})}{q(z|x_{1:m}, y_{1:m})} &\left. \right] + \text{const}. \end{aligned} \quad (4)$$

To learn the NP model, one can maximize this ELBO. Under the setting of SSL, we consider that only labeled data can be treated as context points, and either labeled or unlabeled data can be treated as target points, since the target points are what the NP model makes predictions for.

3.2.2 NP-Match Pipeline

We now introduce the NP-Match pipeline. We first focus on the configuration of the NP model, which is shown in the red dotted box in Figure 1. The NP model is mainly constructed by MLPs, memory banks, and a classifier. Specifically, the classifier is composed of the weight matrix (W) and the softmax function (Φ). Similarly to the original implementation of NPs, we build two paths with the memory banks and MLPs, namely, the latent path and the deterministic path. The decoder $g(\cdot)$ is also implemented with MLPs. The workflow of NP-Match at the training stage and the inference stage are different, which are shown in Figure 1, and they are introduced separately as follows.

Training mode. Given a batch of B labeled images $\mathcal{L} = \{(x_i, y_i) : i \in \{1, \dots, B\}\}$ and a batch of unlabeled images $\mathcal{U} = \{x_i^u : i \in \{1, \dots, \mu B\}\}$ at each iteration, where μ determines the relative size of \mathcal{U} to \mathcal{L} , we apply weak augmentation (i.e., crop-and-flip) on the labeled and unlabeled samples, and strong augmentation (i.e., RandAugment [76]) on only the unlabeled samples. After the augmentation is applied, the images are passed through the deep neural network, and the features are input to the NP model, which finally outputs the predictions and associated uncertainties. The detailed process can be summarized as follows. At the start of each iteration, NP-Match is switched to inference mode, and it makes predictions for the weakly-augmented unlabeled data. Then, inference mode is turned off, and these predictions are treated as pseudo-labels for unlabeled data. After receiving the features, real labels, and pseudo-labels, the NP model first duplicates the labeled samples and treats them as context points, and all the labeled and unlabeled samples in the original batches are then treated as target points, since the NP model needs to make a prediction for them. Thereafter, the target points and context points are separately fed to the latent path and the deterministic path. As for the latent path, target points are concatenated with their corresponding real labels or pseudo labels, and processed by MLPs to get new representations. Then, the representations are averaged by a mean aggregator along the batch dimension, leading to an order-invariant representation, which implements the exchangeability and the consistency condition, and they are simultaneously stored in the latent memory bank, which is updated with a first-in-first-out strategy. After the mean aggregator, the order-invariant representation is further processed by other two MLPs in order to get the mean vector and the variance

vector, which are used for sampling latent vectors via the reparameterization trick, and the number of latent vectors sampled at each feed-forward pass is denoted T . As for the deterministic path, context points are input to this path and are processed in the same way as the target points, until an order-invariant representation is procured from the mean aggregator. We also introduce a memory bank to the deterministic path for storing representations. Subsequently, each target point is concatenated with the T latent vectors and the order-invariant representations from the deterministic path (note that, practically, the target point and the order-invariant representations from the deterministic path must be copied T times). After the concatenation operation, the $T * r$ feature representations are fed into the decoder $g(\cdot)$ and then the classifier, which outputs T probability distributions over classes for each target point. The final prediction for each target point can be obtained by averaging the T predictions, and the uncertainty is computed as the entropy of the average prediction [77]. The ELBO (Eq. (4)) shows the learning objective. Specifically, the first term can be achieved by using the cross-entropy loss on the labeled and unlabeled data with their corresponding real labels and pseudo-labels, while the second term is the KL divergence between $q(z|x_{m+1:m+r}, y_{m+1:m+r})$ and $q(z|x_{1:m}, y_{1:m})$.

Inference mode. Concerning a set of test images, they are also passed through the deep neural network at first to obtain their feature representations. Then, they are treated as target points and are fed to the NP model. Since the labels of test data are not available, it is impossible to obtain the order-invariant representation from test data. In this case, the stored features in the two memory banks can be directly used. As the bottom diagram of Figure 1 shows, after the order-invariant representations are obtained from the memory banks, the target points are leveraged in the same way as in the training mode to generate concatenated feature representations for the decoder $g(\cdot)$ and then the classifier.

3.2.3 Uncertainty-guided Skew-Geometric JS Divergence

NP-Match, like many SSL approaches, relies on the use of pseudo-labels for the unlabeled samples. Pseudo-labels, however, are sometimes inaccurate and can lead to the neural network learning poor feature representations. In our pipeline, this can go on to impact the representation procured from the mean-aggregator and hence the model’s estimated mean vector, variance vector, and global latent vectors (see “Latent Path” in 1). To remedy this, similarly to how the KL divergence term in the ELBO (Eq. (4)) is used to learn global latent variables [25], we propose a new distribution divergence, called the uncertainty-guided skew-geometric JS divergence ($JS^{G\alpha_u}$). We first formalize the definition of $JS^{G\alpha_u}$:

Definition 1. Let (Ω, Σ) be a measurable space, where Ω denotes the sample space, and Σ denotes the σ -algebra of measurable events. P and Q are two probability measures defined on the measurable space. Concerning a positive measure¹, which is

1. Specifically, the positive measure is usually the Lebesgue measure with the Borel σ -algebra $\mathcal{B}(\mathbb{R}^d)$ or the counting measure with the power set σ -algebra 2^Ω .

denoted as μ , the uncertainty-guided skew-geometric JS divergence ($JS^{G_{\alpha_u}}$) can be defined as:

$$JS^{G_{\alpha_u}}(p, q) = (1 - \alpha_u) \int p \log \frac{p}{G(p, q)_{\alpha_u}} d\mu + \alpha_u \int q \log \frac{q}{G(p, q)_{\alpha_u}} d\mu, \quad (5)$$

where p and q are the Radon-Nikodym derivatives of P and Q with respect to μ , the scalar $\alpha_u \in [0, 1]$ is calculated based on the uncertainty, and $G(p, q)_{\alpha_u} = p^{1-\alpha_u} q^{\alpha_u} / (\int_{\Omega} p^{1-\alpha_u} q^{\alpha_u} d\mu)$. The dual form of $JS^{G_{\alpha_u}}$ is given by:

$$JS_*^{G_{\alpha_u}}(p, q) = (1 - \alpha_u) \int G(p, q)_{\alpha_u} \log \frac{G(p, q)_{\alpha_u}}{p} d\mu + \alpha_u \int G(p, q)_{\alpha_u} \log \frac{G(p, q)_{\alpha_u}}{q} d\mu. \quad (6)$$

The proposed $JS^{G_{\alpha_u}}$ is an extension of the skew-geometric JS divergence first proposed by Nielsen et al. [78]. Specifically, Nielsen et al. [78] generalize the JS divergence with abstract means (quasi-arithmetic means [79]), in which a scalar α is defined to control the degree of divergence skew.² By selecting the weighted geometric mean $p^{1-\alpha} q^{\alpha}$, such generalized JS divergence becomes the skew-geometric JS divergence, which can be easily applied to the Gaussian distribution because of its property that the weighted product of exponential family distributions stays in the exponential family [80]. Our $JS^{G_{\alpha_u}}$ extends such divergence by incorporating the uncertainty into the scalar α to dynamically adjust the divergence skew. We assume the real variational distribution of the global latent variable under the supervised learning to be q^* . If the framework is trained with real labels, the condition $q(z|x_{m+1:m+r}, y_{m+1:m+r}) = q(z|x_{1:m}, y_{1:m}) = q^*$ will hold after training, since they are all the marginal distributions of the same stochastic process. However, as for SSL, $q(z|x_{m+1:m+r}, y_{m+1:m+r})$ and $q(z|x_{1:m}, y_{1:m})$ are no longer equal to q^* , as some low-quality representations are involved during training, which affect the estimation of $q(z|x_{m+1:m+r}, y_{m+1:m+r})$ and $q(z|x_{1:m}, y_{1:m})$. Our proposed $JS^{G_{\alpha_u}}$ solves this issue by introducing an intermediate distribution that is calculated via $G(q(z|x_{1:m}, y_{1:m}), q(z|x_{m+1:m+r}, y_{m+1:m+r}))_{\alpha_u}$, where $\alpha_u = u_{c_{avg}} / (u_{c_{avg}} + u_{t_{avg}})$. Here, $u_{c_{avg}}$ denotes the average value over the uncertainties of the predictions of context points, and $u_{t_{avg}}$ represents the average value over that of target points. With this setting, the intermediate distribution is usually close to q^* . For example, when $u_{c_{avg}}$ is large, and $u_{t_{avg}}$ is small, which means that there are many low-quality feature presentations involved for calculating $q(z|x_{1:m}, y_{1:m})$, and $q(z|x_{m+1:m+r}, y_{m+1:m+r})$ is closer to q^* , then $G(q(z|x_{1:m}, y_{1:m}), q(z|x_{m+1:m+r}, y_{m+1:m+r}))_{\alpha_u}$ will be close to $q(z|x_{m+1:m+r}, y_{m+1:m+r})$, and as a result, the network is optimized to learn the distribution of the global latent variable in the direction to q^* , which mitigates the issue to some extent.³ Concerning the variational distribution being supposed to be a Gaussian distribution, we introduce the following theorem (with proof in the supplementary

material) for calculating $JS^{G_{\alpha_u}}$ on Gaussian distributions:

Theorem 1. Given two multivariate Gaussians $\mathcal{N}_1(\mu_1, \Sigma_1)$ and $\mathcal{N}_2(\mu_2, \Sigma_2)$, the following holds:

$$JS^{G_{\alpha_u}}(\mathcal{N}_1, \mathcal{N}_2) = \frac{1}{2} (\text{tr}(\Sigma_{\alpha_u}^{-1}((1 - \alpha_u)\Sigma_1 + \alpha_u\Sigma_2)) + (1 - \alpha_u)(\mu_{\alpha_u} - \mu_1)^T \Sigma_{\alpha_u}^{-1}(\mu_{\alpha_u} - \mu_1) + \alpha_u(\mu_{\alpha_u} - \mu_2)^T \Sigma_{\alpha_u}^{-1}(\mu_{\alpha_u} - \mu_2) + \log \left[\frac{\det[\Sigma_{\alpha_u}]}{\det[\Sigma_1]^{1-\alpha_u} \det[\Sigma_2]^{\alpha_u}} \right] - D) \quad (7)$$

$$JS_*^{G_{\alpha_u}}(\mathcal{N}_1, \mathcal{N}_2) = \frac{1}{2} (\log \left[\frac{\det[\Sigma_1]^{1-\alpha_u} \det[\Sigma_2]^{\alpha_u}}{\det[\Sigma_{\alpha_u}]} \right] + \alpha_u \mu_2^T \Sigma_2^{-1} \mu_2 - \mu_{\alpha_u}^T \Sigma_{\alpha_u}^{-1} \mu_{\alpha_u} + (1 - \alpha_u) \mu_1^T \Sigma_1^{-1} \mu_1),$$

where $\Sigma_{\alpha_u} = ((1 - \alpha_u)\Sigma_1^{-1} + \alpha_u\Sigma_2^{-1})^{-1}$ and $\mu_{\alpha_u} = \Sigma_{\alpha_u}((1 - \alpha_u)\Sigma_1^{-1}\mu_1 + \alpha_u\Sigma_2^{-1}\mu_2)$, D denotes the number of dimension, and $\det[\cdot]$ represents the determinant.

With Theorem 1, one can calculate $JS^{G_{\alpha_u}}$ or its dual form $JS_*^{G_{\alpha_u}}$ based on the mean vector and the variance vector, and use $JS^{G_{\alpha_u}}$ or $JS_*^{G_{\alpha_u}}$ to replace the original KL divergence term in the ELBO (Eq. (4)) for training the whole framework. When the two distributions are diagonal Gaussians, Σ_1 and Σ_2 can be implemented by diagonal matrices with the variance vectors for calculating $JS^{G_{\alpha_u}}$ or $JS_*^{G_{\alpha_u}}$.

3.2.4 Loss Functions

To calculate loss functions, reliable pseudo-labels are required for unlabeled data. In practice, to select reliable unlabeled samples from \mathcal{U} and their corresponding pseudo-labels, we preset a confidence threshold (τ_c) and an uncertainty threshold (τ_u). In particular, as for unlabeled data x_i^u , NP-Match gives its prediction $p(y|Aug_w(x_i^u))$ and associated uncertainty estimate under the inference mode, where $Aug_w(\cdot)$ denotes the weak augmentation. When the highest prediction score $\max(p(y|Aug_w(x_i^u)))$ is higher than τ_c , and the uncertainty is smaller than τ_u , the sample will be chosen, and we denote the selected sample as $x_i^{u_c}$, since the model is certain about his prediction, and the pseudo-label of $x_i^{u_c}$ is $\hat{y}_i = \arg \max(p(y|Aug_w(x_i^{u_c})))$. Concerning μB unlabeled samples in \mathcal{U} , we assume B_c unlabeled samples are selected from them in each feedforward pass. According to the ELBO (Eq. (4)), three loss terms are used for training, namely, L_{cls} , L_{cls}^u , and $JS^{G_{\alpha_u}}$. For each input (labeled or unlabeled), the NP model can give T predictions, and hence L_{cls} and L_{cls}^u are defined as:

$$L_{cls} = \frac{1}{B \times T} \sum_{i=1}^B \sum_{j=1}^T H(y_i^*, p_j(y|Aug_w(x_i))), \quad (8)$$

$$L_{cls}^u = \frac{1}{B_c \times T} \sum_{i=1}^{B_c} \sum_{j=1}^T H(\hat{y}_i, p_j(y|Aug_s(x_i^{u_c}))),$$

where $Aug_s(\cdot)$ denotes the strong augmentation, y_i^* represents the real label for the labeled sample x_i , and $H(\cdot, \cdot)$ denotes the cross-entropy between two distributions. Thus, the total loss function is given by:

$$L_{total} = L_{cls} + \lambda_u L_{cls}^u + \beta JS^{G_{\alpha_u}}, \quad (9)$$

2. The divergence skew means how closely related the intermediate distribution (the abstract mean of p and q) is to p or q .

3. As long as one of $q(z|x_{1:m}, y_{1:m})$ and $q(z|x_{m+1:m+r}, y_{m+1:m+r})$ is close to q^* , the proposed $JS^{G_{\alpha_u}}$ mitigates the issue, but $JS^{G_{\alpha_u}}$ still has difficulties to solve the problem when both of their calculations involve many low-quality representations.

TABLE 1
Comparison with SOTA results on CIFAR-10, CIFAR-100, and STL-10. The error rates are reported with standard deviation.

Dataset	CIFAR-10			CIFAR-100			STL-10			
	Label Amount	40	250	4000	400	2500	10000	40	250	1000
MixMatch [13]		36.19 (± 6.48)	13.63 (± 0.59)	6.66 (± 0.26)	67.59 (± 0.66)	39.76 (± 0.48)	27.78 (± 0.29)	54.93 (± 0.96)	34.52 (± 0.32)	21.70 (± 0.68)
ReMixMatch [14]		9.88 (± 1.03)	6.30 (± 0.05)	4.84 (± 0.01)	42.75 (± 1.05)	26.03 (± 0.35)	20.02 (± 0.27)	32.12 (± 6.24)	12.49 (± 1.28)	6.74 (± 0.14)
UDA [38]		10.62 (± 3.75)	5.16 (± 0.06)	4.29 (± 0.07)	46.39 (± 1.59)	27.73 (± 0.21)	22.49 (± 0.23)	37.42 (± 8.44)	9.72 (± 1.15)	6.64 (± 0.17)
CoMatch [15]		6.88 (± 0.92)	4.90 (± 0.35)	4.06 (± 0.03)	40.02 (± 1.11)	27.01 (± 0.21)	21.83 (± 0.23)	31.77 (± 2.56)	11.56 (± 1.27)	8.66 (± 0.41)
SemCo [16]		7.87 (± 0.22)	5.12 (± 0.27)	3.80 (± 0.08)	44.11 (± 1.18)	31.93 (± 0.33)	24.45 (± 0.12)	34.17 (± 2.78)	12.23 (± 1.40)	7.49 (± 0.29)
Meta Pseudo Labels [10]		6.93 (± 0.17)	4.94 (± 0.04)	3.89 (± 0.07)	44.23 (± 0.99)	27.68 (± 0.22)	22.48 (± 0.18)	34.29 (± 3.29)	9.90 (± 0.96)	6.45 (± 0.26)
FlexMatch [8]		4.96 (± 0.06)	4.98 (± 0.09)	4.19 (± 0.01)	39.94 (± 1.62)	26.49 (± 0.20)	21.90 (± 0.15)	29.15 (± 4.16)	8.23 (± 0.39)	5.77 (± 0.18)
SimMatch [81]		5.63 (± 0.72)	4.50 (± 0.04)	3.97 (± 0.03)	39.29 (± 0.55)	25.21 (± 0.17)	20.63 (± 0.05)	25.13 (± 0.76)	8.72 (± 0.45)	6.11 (± 0.19)
UPS [9]		5.26 (± 0.29)	5.11 (± 0.08)	4.25 (± 0.05)	41.07 (± 1.66)	27.14 (± 0.24)	21.97 (± 0.23)	30.82 (± 2.16)	9.77 (± 0.44)	6.02 (± 0.28)
FixMatch [7]		7.47 (± 0.28)	4.86 (± 0.05)	4.21 (± 0.08)	46.42 (± 0.82)	28.03 (± 0.16)	22.20 (± 0.12)	35.96 (± 4.14)	9.81 (± 1.04)	6.25 (± 0.33)
NP-Match (ours)		4.91 (± 0.04)	4.96 (± 0.06)	4.11 (± 0.02)	38.91 (± 0.99)	26.03 (± 0.26)	21.22 (± 0.13)	14.20 (± 0.67)	9.51 (± 0.37)	5.59 (± 0.24)

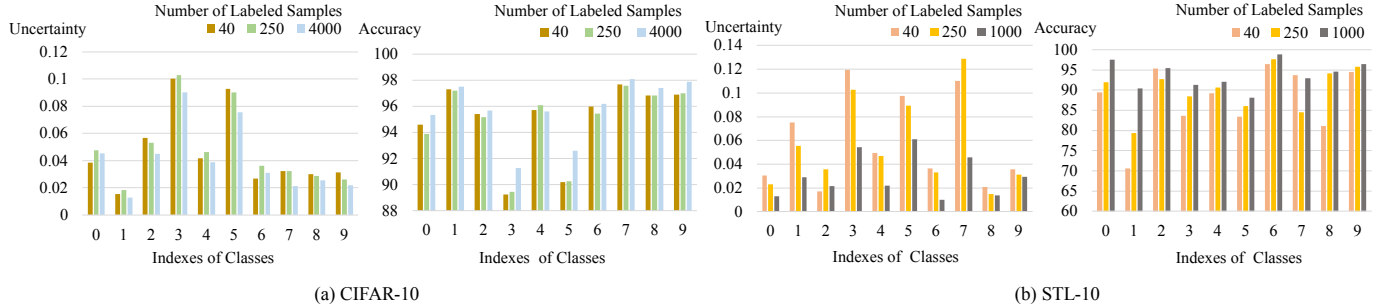


Fig. 2. Analysis of class-wise uncertainty and accuracy on CIFAR-10 and STL-10. For each class, all samples are collected, and their average uncertainty and the accuracy are calculated.

TABLE 2
Expected UCEs (%) of the MC-dropout-based model (i.e., UPS [9]) and of NP-Match on the test sets of CIFAR-10 and STL-10.

Dataset	CIFAR-10			STL-10			
	Label Amount	40	250	4000	40	250	1000
UPS (MC Dropout)		7.96	7.02	5.82	17.23	9.65	5.69
NP-Match		7.23	6.85	5.89	12.45	8.72	5.28

TABLE 3
Error rates of SOTA methods on ImageNet.

	Method	Top-1	Top-5
	Deterministic Methods	FixMatch [7]	43.66
FlexMatch [8]		41.85	19.48
CoMatch [15]		42.17	19.64
Probabilistic Methods	UPS [9]	42.69	20.23
	NP-Match	41.78	19.33

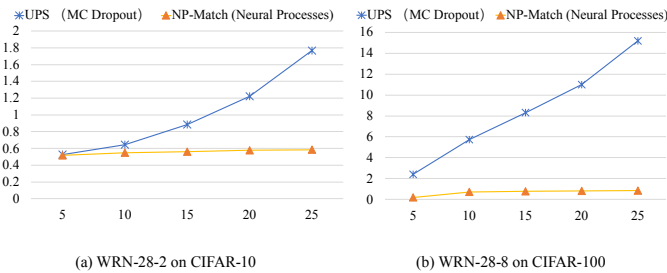


Fig. 3. Time consumption of estimating uncertainty for the MC-dropout-based model (i.e., UPS [9]) and NP-Match. The horizontal axis refers to the number of predictions used for the uncertainty quantification, and the vertical axis indicates the time consumption (sec).

where λ_u and β are coefficients. During training, we followed previous work [7], [8], [9], [15] to utilize the exponential moving average (EMA) technique. Note that, in the implementation, NP-Match only preserves the averaged representation over all representations in each memory bank after training, which just takes up negligible storage space.

4 EXPERIMENTS

We now report our experiments on five public image classification benchmarks under three different semi-supervised image classification settings. For readability, implementation details are given in the supplementary material.

4.1 Datasets

For standard semi-supervised image classification, we conducted our experiments on four widely used public SSL benchmarks, including CIFAR-10 [82], CIFAR-100 [82], STL-10 [83], and ImageNet [84]. CIFAR-10 and CIFAR-100 contain 50,000 images of size 32×32 from 10 and 100 classes, respectively. We evaluated NP-match on these two datasets following the evaluation settings used in previous works [7], [8], [15]. The STL-10 dataset has 5000 labeled samples with size 96×96 from 10 classes and 100,000 unlabeled samples, and it is more difficult than CIFAR, since STL-10 has a number of out-of-distribution images in the unlabeled set. We follow the experimental settings for STL-10 as detailed in [8]. Finally, ImageNet contains around 1.2 million images

TABLE 4

Comparison with SOTA results on long-tailed CIFAR-10 (CIFAR-10-LT) and long-tailed CIFAR-100 (CIFAR-100-LT) under $\gamma_l = \gamma_u$ setup. The accuracy is reported with standard deviation.

Methods	CIFAR-10-LT				CIFAR-100-LT			
	$\gamma = \gamma_l = \gamma_u = 100$		$\gamma = \gamma_l = \gamma_u = 150$		$\gamma = \gamma_l = \gamma_u = 10$		$\gamma = \gamma_l = \gamma_u = 20$	
	$N_1=500$ $M_1=4000$	$N_1=1500$ $M_1=3000$	$N_1=500$ $M_1=4000$	$N_1=1500$ $M_1=3000$	$N_1=50$ $M_1=400$	$N_1=150$ $M_1=300$	$N_1=50$ $M_1=400$	$N_1=150$ $M_1=300$
DARP [55]	74.50 (± 0.78)	77.80 (± 0.63)	67.20 (± 0.32)	73.60 (± 0.73)	49.40 (± 0.20)	58.10 (± 0.44)	43.40 (± 0.87)	52.20 (± 0.66)
CReST [56]	76.30 (± 0.86)	78.10 (± 0.42)	67.50 (± 0.45)	73.70 (± 0.34)	44.50 (± 0.94)	57.40 (± 0.18)	40.10 (± 1.28)	52.10 (± 0.21)
DASO [60]	76.00 (± 0.37)	79.10 (± 0.75)	70.10 (± 1.81)	75.10 (± 0.77)	49.80 (± 0.24)	59.20 (± 0.35)	43.60 (± 0.09)	52.90 (± 0.42)
ABC [59] + DASO [60]	80.10 (± 1.16)	83.40 (± 0.31)	70.60 (± 0.80)	80.40 (± 0.56)	50.20 (± 0.62)	60.00 (± 0.32)	44.50 (± 0.25)	55.30 (± 0.53)
LA [52] + DARP [55]	76.60 (± 0.92)	80.80 (± 0.62)	68.20 (± 0.94)	76.70 (± 1.13)	50.50 (± 0.78)	59.90 (± 0.32)	44.40 (± 0.65)	53.80 (± 0.43)
LA [52] + CReST [56]	76.70 (± 1.13)	81.10 (± 0.57)	70.90 (± 1.18)	77.90 (± 0.71)	44.00 (± 0.21)	57.10 (± 0.55)	40.60 (± 0.55)	52.30 (± 0.20)
LA [52] + DASO [60]	77.90 (± 0.88)	82.50 (± 0.08)	70.10 (± 1.68)	79.00 (± 2.23)	50.70 (± 0.51)	60.60 (± 0.71)	44.10 (± 0.61)	55.10 (± 0.72)
DASO w. UPS [9]	75.44 (± 0.79)	78.11 (± 0.43)	69.64 (± 1.01)	74.39 (± 0.83)	49.16 (± 0.33)	57.87 (± 0.33)	43.02 (± 0.38)	52.23 (± 0.61)
LA + DASO w. UPS [9]	78.89 (± 0.24)	81.24 (± 0.54)	71.39 (± 0.78)	77.83 (± 0.94)	50.04 (± 0.47)	58.92 (± 0.49)	43.95 (± 0.54)	53.98 (± 0.82)
ABC + DASO w. UPS [9]	79.22 (± 0.31)	81.02 (± 0.39)	71.67 (± 0.65)	78.61 (± 0.88)	50.39 (± 0.67)	58.55 (± 0.69)	44.07 (± 0.38)	54.12 (± 0.77)
DASO w. NPs	76.06 (± 0.11)	79.23 (± 0.42)	70.13 (± 1.39)	75.17 (± 0.81)	49.46 (± 0.42)	57.66 (± 0.55)	43.32 (± 0.83)	51.96 (± 0.51)
LA + DASO w. NPs	80.44 (± 0.42)	84.02 (± 0.23)	73.24 (± 0.94)	81.25 (± 0.87)	50.97 (± 0.55)	58.77 (± 0.69)	44.65 (± 0.66)	53.86 (± 0.31)

TABLE 5

Comparison with SOTA methods on long-tailed CIFAR-10 (CIFAR-10-LT) and long-tailed STL-10 (STL-10-LT) under $\gamma_l \neq \gamma_u$ setup. The accuracy is reported with standard deviation.

Methods	CIFAR-10-LT ($\gamma_l \neq \gamma_u$)				STL-10-LT ($\gamma_u = N/A$)			
	$\gamma_u = 1(\text{uniform})$		$\gamma_u = \frac{1}{100}(\text{reversed})$		$\gamma_l = 10$		$\gamma_l = 20$	
	$N_1=500$ $M_1=4000$	$N_1=1500$ $M_1=3000$	$N_1=500$ $M_1=4000$	$N_1=1500$ $M_1=3000$	$N_1=150$ $M_1=100k$	$N_1=450$ $M_1=100k$	$N_1=150$ $M_1=100k$	$N_1=450$ $M_1=100k$
DARP [55]	82.50 (± 0.75)	84.60 (± 0.34)	70.10 (± 0.22)	80.00 (± 0.93)	66.90 (± 1.66)	75.60 (± 0.45)	59.90 (± 2.17)	72.30 (± 0.60)
CReST [56]	82.20 (± 1.53)	86.40 (± 0.42)	62.90 (± 1.39)	72.90 (± 2.00)	61.20 (± 1.27)	71.50 (± 0.96)	56.00 (± 3.19)	68.50 (± 1.88)
DASO [60]	86.60 (± 0.84)	88.80 (± 0.59)	71.00 (± 0.95)	80.30 (± 0.65)	70.00 (± 1.19)	78.40 (± 0.80)	65.70 (± 1.78)	75.30 (± 0.44)
DASO w. UPS [9]	86.32 (± 0.41)	87.94 (± 0.63)	70.62 (± 0.78)	79.59 (± 1.02)	69.04 (± 0.98)	77.74 (± 0.64)	65.10 (± 1.22)	74.03 (± 0.73)
DASO w. NPs	87.50 (± 0.65)	88.21 (± 0.58)	73.87 (± 0.87)	80.42 (± 0.96)	68.45 (± 1.38)	78.53 (± 0.76)	66.98 (± 1.52)	74.05 (± 0.85)

from 1000 classes. Following the experimental settings in [8], we used 100K labeled data, namely, 100 labels per class.

For the imbalanced semi-supervised image classification task, we still chose CIFAR-10 [82], CIFAR-100 [82], and STL-10 [83], but with imbalanced class distribution for both labeled and unlabeled data. By following [60], the imbalanced settings were achieved by exponentially decreasing the number of samples within each class. Specifically, the head class size is denoted as N_1 (M_1) and the imbalance ratio is denoted as γ_l (γ_u) for labeled (unlabeled) data separately, where γ_l and γ_u are independent from each other.

For the multi-label semi-supervised image classification task, we chose a widely-used medical dataset, named Chest X-Ray14. Chest X-Ray14 is a collection of 112,120 chest X-ray images from 30,805 patients, with 14 labels (each label is a disease) and *No Finding* class. Note that each patient can have more than one label, leading to a multi-label classification problem. We employed the official training and testing data split, and we followed [85] to use area under the ROC curve (AUC) as the evaluation metric.

4.2 Main Results

4.2.1 Semi-Supervised Image Classification Experimental Results

In the following, we report the experimental results on the accuracy, the average uncertainty, the expected uncertainty

calibration error, and the running time of NP-Match compared with SOTA approaches.

First, in Table 1, we compare NP-Match with SOTA semi-supervised image classification methods on CIFAR-10, CIFAR-100, and STL-10. We see that NP-Match outperforms SOTA results or achieves competitive results under different SSL settings. We highlight two key observations. First, NP-Match outperforms all other methods by a wide margin on all three benchmarks under the most challenging settings, where the number of labeled samples is smallest. Second, NP-Match is compared to UPS⁴, since the UPS framework is the MC-dropout-based probabilistic model for semi-supervised image classification, and NP-Match completely outperforms them on all three benchmarks. This suggests that NPs can be a good alternative to MC dropout in probabilistic approaches to semi-supervised learning tasks.

Second, we analyse the relationship between the average class-wise uncertainty and accuracy at test phase on CIFAR-10 and STL10. From Figure 2, we empirically observe that: (1) when more labeled data are used for training, the average uncertainty of samples' predictions for each class decreases. This is consistent with the property of NPs and GPs where the model is less uncertain with regard to its prediction when more real and correct labels are leveraged; (2) the classes

4. Note that UPS [9] does not use strong augmentations, thus we re-implemented it with RandAugment [76] for fair comparisons.

TABLE 6

Class-level AUC testing set results comparison on Chest X-Ray14 based on DenseNet-169 [86], under the 20% of labelled data setting. **Bold** number denotes the best result per class and underlined shows second best result in each class.

Method Type	Consistency based			Pseudo-labelling				
	MT [87]	SRC-MT [88]	S^2MTS^2 [89]	GraphXNet [90]	UPS [9]	ACPL [85]	ACPL-UPS	ACPL-NPs
Atelectasis	75.12	75.38	<u>77.45</u>	72.03	76.87	77.25	77.08	77.54
Cardiomegaly	87.37	<u>87.70</u>	86.84	88.21	86.01	84.68	85.26	85.30
Effusion	80.81	81.58	82.11	79.52	81.12	83.13	82.27	<u>82.95</u>
Infiltration	70.67	70.40	70.32	71.64	71.02	<u>71.26</u>	71.04	71.03
Mass	77.72	78.03	82.82	80.29	81.59	81.68	81.79	<u>82.39</u>
Nodule	73.27	73.64	75.29	71.13	76.89	76.00	<u>76.42</u>	75.85
Pneumonia	69.17	69.27	72.66	76.28	71.44	<u>73.66</u>	73.11	72.78
Pneumothorax	85.63	86.12	<u>86.78</u>	84.24	86.02	86.08	86.12	86.80
Consolidation	72.51	73.11	74.21	73.24	<u>74.38</u>	74.48	74.48	74.34
Edema	82.72	82.94	<u>84.23</u>	81.77	82.88	<u>84.23</u>	83.91	84.61
Emphysema	88.16	88.98	91.55	84.89	90.17	<u>92.47</u>	91.99	92.69
Fibrosis	78.24	79.22	81.29	81.25	80.54	81.97	<u>81.55</u>	80.94
Pleural Thickening	74.43	75.63	<u>77.02</u>	76.23	76.13	76.92	76.53	77.05
Hernia	<u>87.74</u>	87.27	85.64	86.89	84.12	84.49	85.10	89.08
Mean	78.83	79.23	80.58	79.12	79.94	<u>80.59</u>	80.48	80.95

with higher average uncertainties have lower accuracy, meaning that the uncertainty is a good standard for choosing unlabeled samples.

Third, the expected uncertainty calibration error (UCE) of our method is also calculated to evaluate the uncertainty estimation. The expected UCE is used to measure the miscalibration of uncertainty [91], which is an analogue to the expected calibration error (ECE) [92], [93]. The low expected UCE indicates that the model is certain when making accurate predictions and that the model is uncertain when making inaccurate predictions. More details about the expected UCE can be found in previous works [91], [94]. The results of NP-Match and the MC-dropout-based model (i.e., UPS [9]) are shown in Table 2; their comparison shows that NP-Match can output more reliable and well-calibrated uncertainty estimates.

Furthermore, we compare the running time of NP-Match and the MC dropout-based model (i.e., UPS [9]). We use a batch of 16 samples and two network architectures that are widely used in previous works [7], [8], [15], [95], namely, WRN-28-2 on CIFAR-10 (Figure 3 (a)) and WRN-28-8 on CIFAR-100 (Figure 3 (b)). In (a), we observe that when the number of predictions (T) increases, the time cost of the UPS framework rises quickly, but the time cost of NP-Match grows slowly. In (b), we observe that the time cost gap between these two methods is even larger when a larger model is tested on a larger dataset. This demonstrates that NP-Match is significantly more computationally efficient than MC dropout-based methods.

Finally, Table 3 shows the experiments conducted on ImageNet. Here, NP-Match achieves a SOTA performance, suggesting that it is effective at handling challenging large-scale datasets. Note that previous works usually evaluate their frameworks under distinct SSL settings, and thus it is hard to compare different methods directly. Therefore, we followed the training details in the previous work [8] due to our limited computational resources, and we also re-evaluate another two methods proposed recently under the same SSL setting with the same training details, namely, UPS and CoMatch.

4.2.2 Imbalanced Semi-Supervised Image Classification Experimental Results

Concerning the imbalanced semi-supervised image classification task, a recent SOTA method called distribution-aware semantics-oriented (DASO) framework [60] is used to validate our method by simply incorporating the NP model into it⁵. We followed the experimental settings in the previous work [60], and the results are shown in Tables 4 and 5. Note that the pipeline of how the NP model generates and selects pseudo-labels for DASO is the same as the descriptions in Section 3.2.2, and therefore, we consider "DASO w. NPs" is the framework that combines NP-Match with DASO for imbalanced semi-supervised image classification. We summarize some findings according to the accuracy from Tables 4 and 5 as follows. First of all, the NP model does not perform well when both labeled and unlabeled data have the same imbalanced distribution, since we can observe minor performance drops in some experimental settings in Table 4 when DASO is equipped with NPs. However, the logit adjustment strategy [52] benefits "DASO w. NPs" more than the original DASO framework, achieving new SOTA results in all imbalanced settings on CIFAR-10 and competitive results on CIFAR-100. Second, concerning another MC-dropout-based probabilistic method for SSL, namely, UPS [9], we combined it with DASO and then found out that it harms the performance in most imbalanced settings. Even though we used two different strategies [52], [59] to rectify the bias towards majority classes, the performance of "DASO w. UPS" is still worse than "DASO w. NPs" in most cases, which demonstrates the meliority of the NP model over UPS and MC dropout for imbalanced semi-supervised image classification. Third, the NP model has a strong capability to handle the situation when the imbalanced distribution of labeled data and that of unlabeled data are different, and as shown in Table 5, it not only improves the accuracy of DASO in most imbalanced settings, but also outperforms UPS [9] by a healthy margin.

5. The details about how the NP model is combined with DASO are shown in the supplementary material.

TABLE 7
Ablation studies of the proposed uncertainty-guided skew-geometric JS divergence and its dual form.

Dataset	CIFAR-10			CIFAR-100			STL-10			
	Label Amount	40	250	4000	400	2500	10000	40	250	1000
NP-Match with KL		5.32 (± 0.06)	5.20 (± 0.02)	4.36 (± 0.03)	39.15 (± 1.53)	26.48 (± 0.23)	21.51 (± 0.17)	14.67 (± 0.38)	9.92 (± 0.24)	6.21 (± 0.23)
NP-Match with $JS_*^{G_{\alpha_u}}$		4.93 (± 0.02)	4.87 (± 0.03)	4.19 (± 0.04)	38.67 (± 1.29)	26.24 (± 0.17)	21.33 (± 0.10)	14.45 (± 0.55)	9.48 (± 0.28)	5.47 (± 0.19)
NP-Match with $JS^{G_{\alpha_u}}$		4.91 (± 0.04)	4.96 (± 0.06)	4.11 (± 0.02)	38.91 (± 0.99)	26.03 (± 0.26)	21.22 (± 0.13)	14.20 (± 0.67)	9.51 (± 0.37)	5.59 (± 0.24)

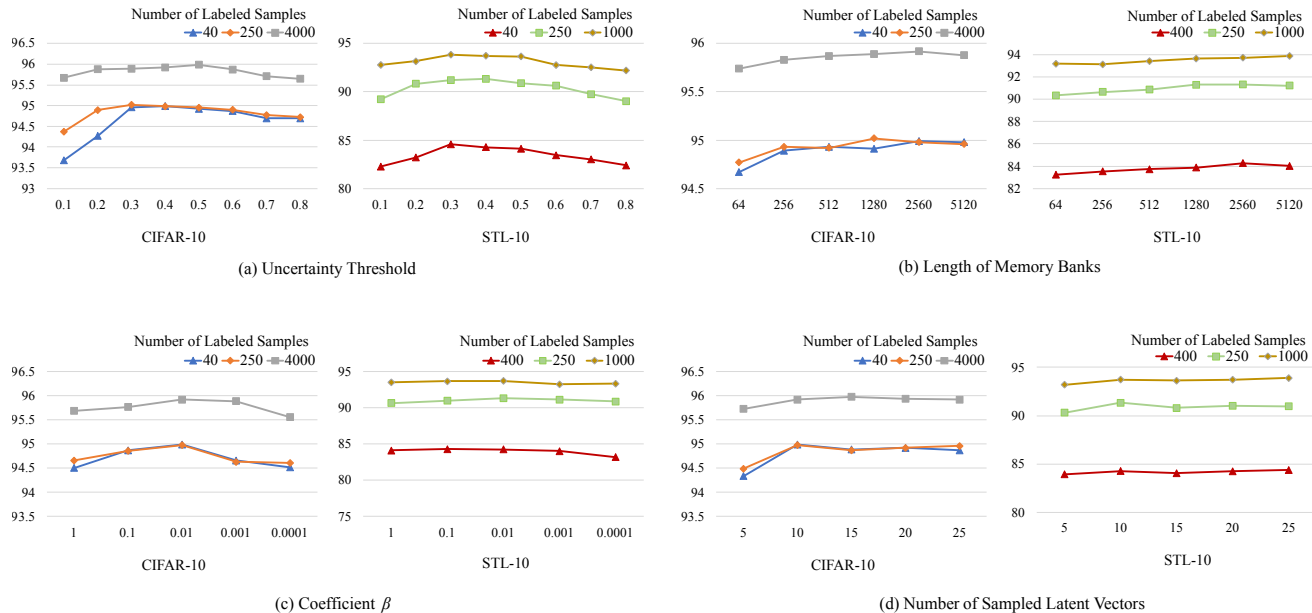


Fig. 4. Performance for different hyperparameters. Four hyperparameters are explored, including the uncertainty threshold (τ_u), the length of memory banks (\mathcal{Q}), the coefficient of $JS^{G_{\alpha_u}}$ (β), and the number of sampled latent vectors (T).

4.2.3 Multi-Label Semi-Supervised Image Classification Experimental Results

We adopted a recent SOTA method, named anti-curriculum pseudo-labelling (ACPL) [85], and integrated our NP model into it⁶, which is denoted as “ACPL-NPs” in Table 6. Similarly, the pipeline of how the NP model generates and selects pseudo-labels for ACPL is also the same as the descriptions in Section 3.2.2, and therefore, we consider “ACPL-NPs” is the framework that combines NP-Match with ACPL for multi-label semi-supervised image classification. For a fair comparison with another probabilistic approach (a.k.a. MC dropout), we combined UPS [9] with ACPL, which is denoted as “ACPL-UPS”.

According to Table 6, we can summarize the following observations. First, after involving the NP model, ACPL-NPs brings a direct improvement over ACPL in terms of the mean AUC, and also outperforms other SOTA methods, indicating that the NP model and our NP-Match pipeline introduces more reliable pseudo-labels for the label ensemble process. Besides, compared against ACPL, ACPL-NPs is able to provide uncertainty estimates, based on which clinicians can further double-check the results in a real-world scenario. Second, compared to ACPL, ACPL-UPS performs worse due to the introduced MC dropout. Concerning that the pseudo-labels from the model are selected based on both confidence

6. The details about how the NP model is combined with ACPL are shown in the supplementary material.

and uncertainty, we empirically consider that the performance drop is caused by the inconsistency between the accuracy and the uncertainty, which is supported by the results in Table 2 to some extent. Third, it is crucial to notice the performance gap between ACPL-NPs and ACPL-UPS, which demonstrates that NP-Match is a superior probabilistic model for SSL.

4.3 Ablation Studies

We only conducted our ablation studies on the standard semi-supervised image classification task, and the results on CIFAR-10, CIFAR-100, and STL-10 are reported. The ablation studies contain two parts. First, we evaluated uncertainty-guided skew-geometric JS divergence and its dual form to verify which one is more suitable for SSL. Second, we did experiments in terms of the hyperparameters related to the NP model in NP-Match, in order to explore how the performance is affected by the changes of hyperparameters, which may provide some hints to readers for applying NP-Match to other datasets.

4.3.1 Uncertainty-guided Skew-geometric JS Divergence

We evaluate our uncertainty-guided skew-geometric JS divergence ($JS^{G_{\alpha_u}}$) as well as its dual form ($JS_*^{G_{\alpha_u}}$), and compare them to the original KL divergence in NPs. In Table 7, we see that NP-Match with KL divergence consistently underperforms relative to our proposed $JS^{G_{\alpha_u}}$

and $JS_*^{G\alpha_u}$. This suggests that our uncertainty-guided skew-geometric JS divergence can mitigate the problem caused by low-quality feature representations. Between the two, $JS^{G\alpha_u}$ and $JS_*^{G\alpha_u}$ achieve a comparable performance across the three benchmarks, and thus we select $JS^{G\alpha_u}$ to replace the original KL divergence in the ELBO (Eq. (4)) for the comparisons to previous SOTA methods in Section 4.2.

4.3.2 Hyperparameter Exploration

For the hyperparameters exploration, we consider four hyperparameters in total, including the uncertainty threshold (τ_u), the length of memory banks (Q), the coefficient of $JS^{G\alpha_u}$ (β), and the number of sampled latent vectors (T). By Figure 4(a), a reasonable τ_u is important. Specifically, lower τ_u usually leads to worse performance, because lower τ_u enforces NP-Match to select a limited number of unlabeled data during training, which is equivalent to training the whole framework with a small dataset. Conversely, when τ_u is too large, more uncertain unlabeled samples are chosen, whose pseudo-labels might be incorrect, and using these uncertain samples to train the framework can also lead to a poor performance. Furthermore, the difficulty of a training set also affects the setting of τ_u , as a more difficult dataset usually has more classes and hard samples (e.g., ImageNet), which makes the uncertainties of predictions large, so that τ_u should be adjusted accordingly. From Figure 4(b), the performance becomes better with the increase of Q . When more context points are used, the more information is involved for inference, and then the NP model can better estimate the global latent variable and make predictions. This observation is consistent with the experimental results where the original NPs are used for image completion [25]. Figure 4(c) shows the ablation study of β that controls the contribution of $JS^{G\alpha_u}$ to the total loss function, and when $\beta = 0.01$, we can obtain the best accuracy on both datasets. By Figure 4(d), if T is smaller than 5, then the performance will go down, but when T is further increased, then the performance of NP-Match is not influenced greatly.

5 SUMMARY AND OUTLOOK

In this work, we proposed the application of neural processes (NPs) to semi-supervised learning (SSL), designing a new framework called NP-Match, and explored its use in semi-supervised large-scale image classification. To our knowledge, this is the first such work. To better adapt NP-Match to the SSL task, we proposed a new divergence term, which we call uncertainty-guided skew-geometric JS divergence, to replace the original KL divergence in NPs. We demonstrated the effectiveness of NP-Match and the proposed divergence term for SSL in extensive experiments, and also showed that NP-Match could be a good alternative to MC dropout in SSL.

Future works will explore the following two directions. First, due to the successful application of NPs to semi-supervised image classification, it is valuable to explore NPs in other SSL tasks, such as object detection and segmentation. Second, many successful NPs variants have been proposed since the original NPs [25] (see Section 2). We will also explore these in SSL for image classification.

ACKNOWLEDGMENTS

This work was partially supported by the Alan Turing Institute under the EPSRC grant EP/N510129/1, by the AXA Research Fund, and by the EPSRC grant EP/R013667/1. We also acknowledge the use of the EPSRC-funded Tier 2 facility JADE (EP/P020275/1) and GPU computing support by Scan Computers International Ltd.

REFERENCES

- [1] A. Krizhevsky, I. Sutskever, and G. E. Hinton, "ImageNet classification with deep convolutional neural networks," in *Proc. Neural Inf. Process. Syst.*, 2012, pp. 1097–1105.
- [2] K. Simonyan and A. Zisserman, "Very deep convolutional networks for large-scale image recognition," in *Proc. Int. Conf. Learn. Representations.*, 2014.
- [3] C. Szegedy, W. Liu, Y. Jia, P. Sermanet, S. Reed, D. Anguelov, D. Erhan, V. Vanhoucke, and A. Rabinovich, "Going deeper with convolutions," in *Proc. IEEE Conf. Comput. Vis. Pattern Recognit.*, 2015, pp. 1–9.
- [4] C. Szegedy, V. Vanhoucke, S. Ioffe, J. Shlens, and Z. Wojna, "Rethinking the inception architecture for computer vision," in *Proc. IEEE Conf. Comput. Vis. Pattern Recognit.*, 2016, pp. 2818–2826.
- [5] K. He, X. Zhang, S. Ren, and J. Sun, "Deep residual learning for image recognition," in *Proc. IEEE Conf. Comput. Vis. Pattern Recognit.*, 2016, pp. 770–778.
- [6] J. Wang and X. Hu, "Convolutional neural networks with gated recurrent connections," *IEEE Trans. Pattern Anal. Mach. Intell.*, 2021.
- [7] K. Sohn, D. Berthelot, C.-L. Li, Z. Zhang, N. Carlini, E. D. Cubuk, A. Kurakin, H. Zhang, and C. Raffel, "FixMatch: Simplifying semi-supervised learning with consistency and confidence," in *Proc. Neural Inf. Process. Syst.*, 2020.
- [8] B. Zhang, Y. Wang, W. Hou, H. Wu, J. Wang, M. Okumura, and T. Shinozaki, "FlexMatch: Boosting semi-supervised learning with curriculum pseudo labeling," in *Proc. Neural Inf. Process. Syst.*, 2021.
- [9] M. N. Rizve, K. Duarte, Y. S. Rawat, and M. Shah, "In defense of pseudo-labeling: An uncertainty-aware pseudo-label selection framework for semi-supervised learning," in *Proc. Int. Conf. Learn. Representations.*, 2021.
- [10] H. Pham, Z. Dai, Q. Xie, and Q. V. Le, "Meta pseudo labels," in *Proc. IEEE Conf. Comput. Vis. Pattern Recognit.*, 2021, pp. 11 557–11 568.
- [11] Y.-F. Li and Z.-H. Zhou, "Towards making unlabeled data never hurt," *IEEE Trans. Pattern Anal. Mach. Intell.*, vol. 37, no. 1, pp. 175–188, 2014.
- [12] W. Liu, J. He, and S.-F. Chang, "Large graph construction for scalable semi-supervised learning," in *Proc. Int. Conf. Mach. Learn.*, 2010.
- [13] D. Berthelot, N. Carlini, I. Goodfellow, N. Papernot, A. Oliver, and C. Raffel, "MixMatch: A holistic approach to semi-supervised learning," in *Proc. Neural Inf. Process. Syst.*, 2019.
- [14] D. Berthelot, N. Carlini, E. D. Cubuk, A. Kurakin, K. Sohn, H. Zhang, and C. Raffel, "ReMixMatch: Semi-supervised learning with distribution alignment and augmentation anchoring," in *Proc. Int. Conf. Learn. Representations.*, 2020.
- [15] J. Li, C. Xiong, and S. C. Hoi, "CoMatch: Semi-supervised learning with contrastive graph regularization," in *Proc. Int. Conf. Comput. Vis.*, 2021, pp. 9475–9484.
- [16] I. Nassar, S. Herath, E. Abbasnejad, W. Buntine, and G. Haffari, "All labels are not created equal: Enhancing semi-supervision via label grouping and co-training," in *Proc. IEEE Conf. Comput. Vis. Pattern Recognit.*, 2021, pp. 7241–7250.
- [17] Z. Hu, Z. Yang, X. Hu, and R. Nevatia, "SimPLE: Similar pseudo label exploitation for semi-supervised classification," in *Proc. IEEE Conf. Comput. Vis. Pattern Recognit.*, 2021, pp. 15 099–15 108.
- [18] Y. Gal and Z. Ghahramani, "Dropout as a Bayesian approximation: Representing model uncertainty in deep learning," in *Proc. Int. Conf. Mach. Learn.*. PMLR, 2016, pp. 1050–1059.
- [19] S. Sedai, B. Antony, R. Rai, K. Jones, H. Ishikawa, J. Schuman, W. Gadi, and R. Garnavi, "Uncertainty guided semi-supervised segmentation of retinal layers in OCT images," in *Int. Conf. on Med. Image Comput. and Comput. Assist. Intervent.* Springer, 2019, pp. 282–290.
- [20] Y. Shi, J. Zhang, T. Ling, J. Lu, Y. Zheng, Q. Yu, L. Qi, and Y. Gao, "Inconsistency-aware uncertainty estimation for semi-supervised medical image segmentation," *IEEE Trans. Med. Imag.*, 2021.

- [21] K. Wang, B. Zhan, C. Zu, X. Wu, J. Zhou, L. Zhou, and Y. Wang, "Tripled-uncertainty guided mean teacher model for semi-supervised medical image segmentation," in *Int. Conf. on Med. Image Comput. and Comput. Assist. Intervent.* Springer, 2021, pp. 450–460.
- [22] L. Yu, S. Wang, X. Li, C.-W. Fu, and P.-A. Heng, "Uncertainty-aware self-ensembling model for semi-supervised 3D left atrium segmentation," in *Int. Conf. on Med. Image Comput. and Comput. Assist. Intervent.* Springer, 2019, pp. 605–613.
- [23] H. Zhu, Y. Li, F. Bai, W. Chen, X. Li, J. Ma, C. S. Teo, P. Y. Tao, and W. Lin, "Grasping detection network with uncertainty estimation for confidence-driven semi-supervised domain adaptation," in *Int. Conf. on Intell. Robot. and Syst.* IEEE, 2020, pp. 9608–9613.
- [24] J. Wang and T. Lukasiewicz, "Rethinking Bayesian deep learning methods for semi-supervised volumetric medical image segmentation," in *Proc. IEEE Conf. Comput. Vis. Pattern Recognit.*, 2022, pp. 182–190.
- [25] M. Garnelo, J. Schwarz, D. Rosenbaum, F. Viola, D. J. Rezende, S. Eslami, and Y. W. Teh, "Neural processes," *arXiv:1807.01622*, 2018.
- [26] V. Sindhwani, W. Chu, and S. S. Keerthi, "Semi-supervised Gaussian process classifiers," in *Int. Joint Conf. on Artif. Intell.*, 2007, pp. 1059–1064.
- [27] N. Jean, S. M. Xie, and S. Ermon, "Semi-supervised deep kernel learning: Regression with unlabeled data by minimizing predictive variance," in *Proc. Neural Inf. Process. Syst.*, 2018.
- [28] R. Yasarla, V. A. Sindagi, and V. M. Patel, "Syn2Real transfer learning for image deraining using Gaussian processes," in *Proc. IEEE Conf. Comput. Vis. Pattern Recognit.*, 2020, pp. 2726–2736.
- [29] J. Wang, T. Lukasiewicz, D. Massiceti, X. Hu, V. Pavlovic, and A. Neophytou, "NP-Match: When neural processes meet semi-supervised learning," in *Proc. Int. Conf. Mach. Learn.* PMLR, 2022, pp. 22919–22934.
- [30] S. Qiao, W. Shen, Z. Zhang, B. Wang, and A. Yuille, "Deep co-training for semi-supervised image recognition," in *Proc. Eur. Conf. Comput. Vis.*, 2018, pp. 135–152.
- [31] D.-D. Chen, W. Wang, W. Gao, and Z.-H. Zhou, "Tri-net for semi-supervised deep learning," in *Int. Joint Conf. on Artif. Intell.*, 2018, pp. 2014–2020.
- [32] D.-H. Lee, "Pseudo-label: The simple and efficient semi-supervised learning method for deep neural networks," in *Proc. Int. Conf. Learn. Representations., Workshop on Challenges in Representation Learning*, vol. 3, 2013, p. 896.
- [33] X. Zhai, A. Oliver, A. Kolesnikov, and L. Beyer, "S4L: Self-supervised semi-supervised learning," in *Proc. Int. Conf. Comput. Vis.*, 2019, pp. 1476–1485.
- [34] X. Wang, D. Kihara, J. Luo, and G.-J. Qi, "EnAET: A self-trained framework for semi-supervised and supervised learning with ensemble transformations," *IEEE Trans. Image Process.*, vol. 30, pp. 1639–1647, 2020.
- [35] P. Bachman, O. Alsharif, and D. Precup, "Learning with pseudo-ensembles," in *Proc. Neural Inf. Process. Syst.*, 2014, pp. 3365–3373.
- [36] M. Sajjadi, M. Javanmardi, and T. Tasdizen, "Regularization with stochastic transformations and perturbations for deep semi-supervised learning," in *Proc. Neural Inf. Process. Syst.*, 2016, pp. 1163–1171.
- [37] S. Laine and T. Aila, "Temporal ensembling for semi-supervised learning," in *Proc. Int. Conf. Learn. Representations.*, 2017.
- [38] Q. Xie, Z. Dai, E. Hovy, M.-T. Luong, and Q. V. Le, "Unsupervised data augmentation for consistency training," in *Proc. Neural Inf. Process. Syst.*, 2020.
- [39] J. Wang, T. Lukasiewicz, X. Hu, J. Cai, and Z. Xu, "RSG: A simple but effective module for learning imbalanced datasets," in *Proc. IEEE Conf. Comput. Vis. Pattern Recognit.*, 2021, pp. 3784–3793.
- [40] J. Cui, Z. Zhong, S. Liu, B. Yu, and J. Jia, "Parametric contrastive learning," in *Proc. Int. Conf. Comput. Vis.*, 2021, pp. 715–724.
- [41] Z. Liu, Z. Miao, X. Zhan, J. Wang, B. Gong, and S. X. Yu, "Large-scale long-tailed recognition in an open world," in *Proc. IEEE Conf. Comput. Vis. Pattern Recognit.*, 2019, pp. 2537–2546.
- [42] T. Li, L. Wang, and G. Wu, "Self supervision to distillation for long-tailed visual recognition," in *Proc. Int. Conf. Comput. Vis.*, 2021, pp. 630–639.
- [43] K. Cao, C. Wei, A. Gaidon, N. Arechiga, and T. Ma, "Learning imbalanced datasets with label-distribution-aware margin loss," *Proc. Neural Inf. Process. Syst.*, vol. 32, 2019.
- [44] Y. Hong, S. Han, K. Choi, S. Seo, B. Kim, and B. Chang, "Disentangling label distribution for long-tailed visual recognition," in *Proc. IEEE Conf. Comput. Vis. Pattern Recognit.*, 2021, pp. 6626–6636.
- [45] C. Feng, Y. Zhong, and W. Huang, "Exploring classification equilibrium in long-tailed object detection," in *Proc. Int. Conf. Comput. Vis.*, 2021, pp. 3417–3426.
- [46] J. Cai, Y. Wang, and J.-N. Hwang, "ACE: Ally complementary experts for solving long-tailed recognition in one-shot," in *Proc. Int. Conf. Comput. Vis.*, 2021, pp. 112–121.
- [47] D. Samuel and G. Chechik, "Distributional robustness loss for long-tail learning," in *Proc. Int. Conf. Comput. Vis.*, 2021, pp. 9495–9504.
- [48] A. Desai, T.-Y. Wu, S. Tripathi, and N. Vasconcelos, "Learning of visual relations: The devil is in the tails," in *Proc. Int. Conf. Comput. Vis.*, 2021, pp. 15404–15413.
- [49] Z. Hou, B. Yu, and D. Tao, "BatchFormer: Learning to explore sample relationships for robust representation learning," in *Proc. IEEE Conf. Comput. Vis. Pattern Recognit.*, 2022.
- [50] J. Li, Z. Tan, J. Wan, Z. Lei, and G. Guo, "Nested collaborative learning for long-tailed visual recognition," in *Proc. IEEE Conf. Comput. Vis. Pattern Recognit.*, 2022, pp. 6949–6958.
- [51] Z. Zhong, J. Cui, S. Liu, and J. Jia, "Improving calibration for long-tailed recognition," in *Proc. IEEE Conf. Comput. Vis. Pattern Recognit.*, 2021, pp. 16489–16498.
- [52] A. K. Menon, S. Jayasumana, A. S. Rawat, H. Jain, A. Veit, and S. Kumar, "Long-tail learning via logit adjustment," in *Proc. Int. Conf. Learn. Representations.*, 2021.
- [53] Y. Yang and Z. Xu, "Rethinking the value of labels for improving class-imbalanced learning," in *Proc. Neural Inf. Process. Syst.*, 2020, pp. 19290–19301.
- [54] M. Hyun, J. Jeong, and N. Kwak, "Class-imbalanced semi-supervised learning," *arXiv:2002.06815*, 2020.
- [55] J. Kim, Y. Hur, S. Park, E. Yang, S. J. Hwang, and J. Shin, "Distribution aligning refinery of pseudo-label for imbalanced semi-supervised learning," in *Proc. Neural Inf. Process. Syst.*, 2020, pp. 14567–14579.
- [56] C. Wei, K. Sohn, C. Mellina, A. Yuille, and F. Yang, "CREST: A class-rebalancing self-training framework for imbalanced semi-supervised learning," in *Proc. IEEE Conf. Comput. Vis. Pattern Recognit.*, 2021, pp. 10857–10866.
- [57] B. Kang, S. Xie, M. Rohrbach, Z. Yan, A. Gordo, J. Feng, and Y. Kalantidis, "Decoupling representation and classifier for long-tailed recognition," in *Proc. Int. Conf. Learn. Representations.*, 2020.
- [58] J. He, A. Kortylewski, S. Yang, S. Liu, C. Yang, C. Wang, and A. Yuille, "Rethinking re-sampling in imbalanced semi-supervised learning," *arXiv:2106.00209*, 2021.
- [59] H. Lee, S. Shin, and H. Kim, "ABC: Auxiliary balanced classifier for class-imbalanced semi-supervised learning," in *Proc. Neural Inf. Process. Syst.*, vol. 34, 2021, pp. 7082–7094.
- [60] Y. Oh, D.-J. Kim, and I. S. Kweon, "DASO: Distribution-aware semantics-oriented pseudo-label for imbalanced semi-supervised learning," in *Proc. IEEE Conf. Comput. Vis. Pattern Recognit.*, 2022, pp. 9786–9796.
- [61] A. G. Wilson, Z. Hu, R. Salakhutdinov, and E. P. Xing, "Deep kernel learning," in *Int. Conf. on Artif. Intell. and Stat.* PMLR, 2016, pp. 370–378.
- [62] O. Ronneberger, P. Fischer, and T. Brox, "U-Net: Convolutional networks for biomedical image segmentation," in *Int. Conf. on Med. Image Comput. and Comput. Assist. Intervent.* Springer, 2015, pp. 234–241.
- [63] Y. C. Ng, N. Colombo, and R. Silva, "Bayesian semi-supervised learning with graph Gaussian processes," in *Proc. Neural Inf. Process. Syst.*, 2018.
- [64] I. Walker and B. Glocker, "Graph convolutional Gaussian processes," in *Proc. Int. Conf. Mach. Learn.* PMLR, 2019, pp. 6495–6504.
- [65] Z.-Y. Liu, S.-Y. Li, S. Chen, Y. Hu, and S.-J. Huang, "Uncertainty aware graph Gaussian process for semi-supervised learning," in *Proc. AAAI Conf. Artif. Intell.*, 2020, pp. 4957–4964.
- [66] M. Garnelo, D. Rosenbaum, C. Maddison, T. Ramalho, D. Saxton, M. Shanahan, Y. W. Teh, D. Rezende, and S. A. Eslami, "Conditional neural processes," in *Proc. Int. Conf. Mach. Learn.* PMLR, 2018, pp. 1704–1713.
- [67] H. Kim, A. Mnih, J. Schwarz, M. Garnelo, A. Eslami, D. Rosenbaum, O. Vinyals, and Y. W. Teh, "Attentive neural processes," in *Proc. Int. Conf. Learn. Representations.*, 2019.
- [68] J. Gordon, W. P. Bruinsma, A. Y. Foong, J. Requeima, Y. Dubois, and R. E. Turner, "Convolutional conditional neural processes," in *Proc. Int. Conf. Learn. Representations.*, 2020.

- [69] C. Louizos, X. Shi, K. Schutte, and M. Welling, "The functional neural process," in *Proc. Neural Inf. Process. Syst.*, 2019.
- [70] J. Lee, Y. Lee, J. Kim, E. Yang, S. J. Hwang, and Y. W. Teh, "Bootstrapping neural processes," in *Proc. Neural Inf. Process. Syst.*, 2020, pp. 6606–6615.
- [71] G. Singh, J. Yoon, Y. Son, and S. Ahn, "Sequential neural processes," in *Proc. Neural Inf. Process. Syst.*, 2019.
- [72] J. Yoon, G. Singh, and S. Ahn, "Robustifying sequential neural processes," in *Proc. Int. Conf. Mach. Learn.* PMLR, 2020, pp. 10 861–10 870.
- [73] J. Requeima, J. Gordon, J. Bronskill, S. Nowozin, and R. E. Turner, "Fast and flexible multi-task classification using conditional neural adaptive processes," in *Proc. Neural Inf. Process. Syst.*, 2019, pp. 7959–7970.
- [74] S. Qin, J. Zhu, J. Qin, W. Wang, and D. Zhao, "Recurrent attentive neural process for sequential data," in *Proc. Neural Inf. Process. Syst., LIRE Workshop*, 2019.
- [75] B. Øksendal, "Stochastic differential equations," in *Stoch. Differ. Equ.* Springer, 2003, pp. 65–84.
- [76] E. D. Cubuk, B. Zoph, J. Shlens, and Q. V. Le, "RandAugment: Practical automated data augmentation with a reduced search space," in *Proc. IEEE Conf. Comput. Vis. Pattern Recognit. Workshops*, 2020, pp. 702–703.
- [77] A. Kendall and Y. Gal, "What uncertainties do we need in Bayesian deep learning for computer vision?" *Proc. Neural Inf. Process. Syst.*, 2017.
- [78] F. Nielsen, "On a generalization of the Jensen-Shannon divergence and the Jensen-Shannon centroid," *Entropy*, vol. 22, no. 2, p. 221, 2020.
- [79] C. Niculescu and L.-E. Persson, *Convex functions and their applications*. Springer, 2006.
- [80] F. Nielsen and V. Garcia, "Statistical exponential families: A digest with flash cards," *arXiv:0911.4863*, 2009.
- [81] M. Zheng, S. You, L. Huang, F. Wang, C. Qian, and C. Xu, "SimMatch: Semi-supervised learning with similarity matching," in *Proc. IEEE Conf. Comput. Vis. Pattern Recognit.*, 2022, pp. 14 471–14 481.
- [82] A. Krizhevsky, "Learning multiple layers of features from tiny images," 2009.
- [83] A. Coates, A. Ng, and H. Lee, "An analysis of single-layer networks in unsupervised feature learning," in *Int. Conf. on Artif. Intell. and Stat.* JMLR Workshop and Conference Proceedings, 2011, pp. 215–223.
- [84] J. Deng, W. Dong, R. Socher, L.-J. Li, K. Li, and L. Fei-Fei, "ImageNet: A large-scale hierarchical image database," in *Proc. IEEE Conf. Comput. Vis. Pattern Recognit.*, 2009, pp. 248–255.
- [85] F. Liu, Y. Tian, Y. Chen, Y. Liu, V. Belagiannis, and G. Carneiro, "ACPL: Anti-curriculum pseudo-labelling for semi-supervised medical image classification," in *Proc. IEEE Conf. Comput. Vis. Pattern Recognit.*, 2022, pp. 20 697–20 706.
- [86] G. Huang, Z. Liu, L. Van Der Maaten, and K. Q. Weinberger, "Densely connected convolutional networks," in *Proc. IEEE Conf. Comput. Vis. Pattern Recognit.*, 2017, pp. 4700–4708.
- [87] A. Tarvainen and H. Valpola, "Mean teachers are better role models: Weight-averaged consistency targets improve semi-supervised deep learning results," in *Proc. Neural Inf. Process. Syst.*, vol. 30, 2017.
- [88] Q. Liu, L. Yu, L. Luo, Q. Dou, and P. A. Heng, "Semi-supervised medical image classification with relation-driven self-ensembling model," *IEEE Trans. Med. Imag.*, vol. 39, no. 11, pp. 3429–3440, 2020.
- [89] F. Liu, Y. Tian, F. R. Cordeiro, V. Belagiannis, I. Reid, and G. Carneiro, "Self-supervised mean teacher for semi-supervised chest x-ray classification," in *Int. Conf. on Med. Image Comput. and Comput. Assist. Intervent. Workshops*. Springer, 2021, pp. 426–436.
- [90] A. I. Aviles-Rivero, N. Papadakis, R. Li, P. Sellars, Q. Fan, R. T. Tan, and C.-B. Schönlieb, "GraphXNET — Chest X-ray classification under extreme minimal supervision," in *Int. Conf. on Med. Image Comput. and Comput. Assist. Intervent.*, D. Shen, T. Liu, T. M. Peters, L. H. Staib, C. Essert, S. Zhou, P.-T. Yap, and A. Khan, Eds. Springer International Publishing, 2019.
- [91] M.-H. Laves, S. Ihler, K.-P. Kortmann, and T. Ortmaier, "Calibration of model uncertainty for dropout variational inference," *arXiv:2006.11584*, 2020.
- [92] C. Guo, G. Pleiss, Y. Sun, and K. Q. Weinberger, "On calibration of modern neural networks," in *Proc. Int. Conf. Mach. Learn.* PMLR, 2017, pp. 1321–1330.
- [93] M. P. Naeni, G. Cooper, and M. Hauskrecht, "Obtaining well calibrated probabilities using Bayesian binning," in *Proc. AAAI Conf. Artif. Intell.*, 2015.
- [94] R. Krishnan and O. Tickoo, "Improving model calibration with accuracy versus uncertainty optimization," *Proc. Neural Inf. Process. Syst.*, 2020.
- [95] S. Zagoruyko and N. Komodakis, "Wide residual networks," *Proc. British Mach. Vis. Conf.*, 2016.